Synthesis, sintering, and thermoelectric properties of Co1-M O (M = Na, 0 ≤ x ≤ 0.07; M = Ag, 0 ≤ x ≤ 0.05)

Cong Chen, Fabian Delorme, Frédéric Schoenstein, Mustapha Zaghrioui, Delphine Flahaut, Joachim Allouche, Fabien Giovannelli

Synthesis, sintering, and thermoelectric properties of $Co_{1-x}M_xO$ (M = Na, $0 \leq x \leq 0.07$; M = Ag, $0 \leq x \leq 0.05$)

Cong Chen[1,2,*], Fabian Delorme[1], Frédéric Schoenstein[3], Mustapha Zaghrioui[1], Delphine Flahaut[4], Joachim Allouche[4], and Fabien Giovannelli[1]

[1] Université de Tours, CNRS, INSA, GREMAN UMR 7347, IUT de Blois, 15 rue de la chocolaterie, CS 2903, 41029 Blois Cedex, France

[2] Bundesanstalt für Materialforschung und –prüfung (BAM), Unter den Eichen 87, 12205 Berlin, Germany

[3] Laboratoire des Sciences des Procédés et des Matériaux, CNRS, LSPM – UPR 3407, Université Paris 13, Sorbonne Paris Cité, 99 Avenue J.B. Clément, 93430 Villetaneuse, France

[4] CNRS/ UNIV PAU & PAYS ADOUR/ E2S UPPA, Insitut des Sciences Analytiques et de Physico-Chimie pour l'Environnement et les Materiaux, UMR5254, 64000, Pau, France

*Corresponding author. Email: saracongchen@gmail.com

Abstract

The structural and thermoelectric properties of Na- and Ag-substituted CoO dense ceramics have been investigated. X-ray diffraction shows that pure phase and Ag/CoO composites have been obtained for Na-doped and Ag-doped CoO, respectively. Raman spectroscopy shows an effect of Na dopants on the lattice disorder of CoO. The chemical composition, element distribution, and valence states of the samples have been characterized by Auger electron microscopy and X-ray photoelectron spectroscopy. Substitution of Co by 5 at. % Na enhances the power factor to 250 $\mu W.m^{-1}.K^{-2}$ at 1000 K, similar to that of $Ca_3Co_4O_9$. The corresponding thermal conductivity is also reduced to 3.55 $W.m^{-1}.K^{-1}$ at 1000 K. Consequently, $Co_{0.95}Na_{0.05}O$ exhibits the best thermoelectric figure of merit (*ZT*), which is 0.07 at 1000 K. On the other hand, the substitution of Ag into CoO leads to the formation of CoO/Ag composites and deteriorates *ZT* values.

Keywords: CoO; Substitution; Spark plasma sintering; XPS; Thermoelectrics

Introduction

In the last three decades, there has been a continuous interest in the search for new thermoelectric materials with enhanced thermoelectric properties. For a thermoelectric device, a high conversion efficiency requires a high figure of merit (*ZT*), $ZT = S^2\sigma T/\kappa$, where *S* is the Seebeck coefficient, σ is the electrical conductivity, *T* is the absolute temperature, and κ is the thermal conductivity. Unfortunately, the classical thermoelectric materials (BiTe, PbTe, SiGe, etc. [1]) show drawbacks like high toxicity, low abundance, high cost, and low chemical stability in air. Although thermoelectric materials with complex crystal structures like skutterudites and clathrates have been identified to show promising *ZT*

[2, 3], they present similar disadvantages as the classical thermoelectric materials. Therefore, oxides without the aforementioned shortcomings are being explored for thermoelectric application.

Single-crystalline layered cobalt oxides present the best *ZT* values among the p-type thermoelectric oxides. A *ZT* value around 1 at high temperature (700 K – 1000 K) has been found in bulk single-crystalline Na_xCoO_2 [4] and $Ca_3Co_4O_9$ [5] as well as in single-crystalline $Bi_2Sr_2Co_2O_y$ whiskers [6]. Each of these materials exhibit similar crystal structures, with CdI_2-type CoO_2 layers separated by Na ions, triple rock-salt $[Ca_2CoO_3]$ layers, and four rock-salt $[Sr_2Bi_2O_4]$ layers, respectively. Reduced *ZT* values have been observed in their corresponding polycrystalline samples due to the grain boundaries and their highly anisotropic crystal structures [4, 7, 8]. Various approaches have been adopted to improve the *ZT* of polycrystalline oxides, for example, doping [9-11] and adding a secondary phase to form composites [7, 12, 13]. The most pronounced enhancement is achieved in $Ca_{2.5}Tb_{0.5}Co_4O_9$, with a highest $ZT \sim 0.74$ at 800 K [14].

These layered cobalt oxides present some unique features. Their large Seebeck coefficient originates from the mixed valence states of low spin states of Co^{3+} and Co^{4+} in the CoO_2 layers [15]. Their low thermal conductivity results from the disordered or misfit block layers in between the CoO_2 layers. In addition to the layered cobalt oxides, acceptor-doped $LaCoO_3$ perovskites show high *ZT* at room temperature [16-18]. In these cobalt oxides, the transport properties are dominated by small polaron hopping between the mixed-valence Co^{3+}/Co^{4+}, which is formed as a result of charge neutralization of dopants. In a recent paper, Delorme et al. [19] have shown that p-type promising thermoelectric performance can be found in $Ba_2Co_9O_{14}$, a layered cobalt oxide with CdI_2-type CoO_2 layers containing a mixed valence of Co^{2+} and Co^{3+} rather than Co^{3+} and Co^{4+}. Finally, NiO ceramics doped with monovalent cations exhibit remarkably enhanced electrical conductivity and *ZT* values compared with undoped NiO [20]. Mixed valency of Ni^{2+}/Ni^{3+} is introduced by dopants to neutralize the dopants and influences the transport properties of NiO.

Here, we propose to study the thermoelectric properties of monovalent-cation-doped CoO, in which the presence of a mixed Co^{2+}/Co^{3+} is expected. Indeed, CoO and NiO show similar crystal structures and electronic structures. CoO has a cubic rock salt crystal structure (Fm-3m) in paramagnetic state and is electrically insulating. Over the past few decades, CoO has been widely studied in terms of nanoparticle synthesis [21-24], electrical and magnetic properties [25-34], defect structure [35-38], etc. Numerous studies on the electrical conduction mechanism in CoO reveal contradictory results, suggesting that the behavior is dominated by either small polaron hopping [25-29, 31] or by band-like conduction [32-34]. A major defect in CoO is cation deficiency on the Co lattice site, which is dependent on the temperature and oxygen partial pressure [30, 35, 38]. The presence of Co^{3+} is possible as cobalt vacancies can be either uncharged or charged. Moreover, the concentration of Co^{3+} can also be tuned by doping monovalent cations into Co^{2+} sites due to charge neutralization. In this work, the proposed compositions are $Co_{1-x}Na_xO$ with $0 \leq x \leq 0.07$ and $Co_{1-x}Ag_xO$ with $0 \leq x \leq 0.05$.

Experiment

$Co_{1-x}Na_xO$ (x = 0, 0.01, 0.03, 0.05, and 0.07) powders were prepared by heat treatment. Prior to the heat treatment, stoichiometric amounts of Co_3O_4 (Sigma Aldrich, no specified purity) and Na_2CO_3 (Chempur, ≥ 99.9%) were mixed at 250 rpm for 5 min in a tungsten carbide ball mill (Retsch PM 100). The powders were then treated at 1223 K for 2 h under a N_2 atmosphere in an alumina crucible. After heat treatment, the synthesized powders were ball milled again.

The $Co_{1-x}Ag_xO$ (x = 0.01 and 0.05) powders used Co_3O_4 (Sigma Aldrich, no specified purity) and Ag_2O (Sigma Aldrich, ≥ 99.99%) as precursor powders. For the composition with x = 0.01, the precursor powders were mixed by ball milling followed by heat treatment with the same parameters as those used for the preparation for the Na-doped CoO. The synthesized powder was then ball milled again. For the composition with x = 0.05, only Co_3O_4 was heated at 1223 K for 2 h in N_2. Then the obtained CoO was mixed with Ag_2O by subsequent ball milling.

Sintering was performed by spark plasma sintering (SPS, Syntex 515 S). The synthesized powder was placed in a 15-mm-diameter graphite die and SPS was carried out in an Ar atmosphere. Different SPS temperatures and dwell times were employed to sinter the undoped CoO in order to achieve a high relative density. Finally, dense CoO was obtained with a sintering temperature of 1273 K, while the Na- and Ag-doped CoO were sintered at 1223 K. The samples were raised to the sintering temperature at a rate of 100 $K.min^{-1}$, dwelled for 10 min under a pressure of 100 MPa, and finally cooled to room temperature at 100 $K.min^{-1}$. Bulk density was determined from the dry mass and the geometric dimensions of the pellets.

X-ray diffraction (XRD) was performed both on the powders after heat treatment and the pellets after SPS. Room temperature XRD patterns were collected using a BRUKER D8 Advance θ/2θ diffractometer equipped with a Linxeye energy-dispersive one-dimensional detector, with Cu-Kα radiation and operating at 40 kV and 40 mA. The patterns were recorded from 20° to 85° (2θ) with a step of 0.02° and a counting time of 1 s per step. The results were analysed by the Rietveld refinement method, using the FullProf Suite program [39].

The sodium content in $Co_{1-x}Na_xO$ ceramics was determined by flame atomic absorption spectroscopy (PerkinElmer AAnalyst 400). Micro-Raman measurements were carried out at both 80 K and room temperature using a Renishaw Invia spectrometer and temperature controller (Linkam THMS 600). A He-Ne laser with a wavelength of 633 nm and a power of 3 mW was used as the excitation light source. A scanning electron microscope (SEM, Tescan MIRA3) equipped with a backscattered electron detector (BSD) and an Energy-dispersive X-ray spectroscopy (EDS, Oxford INCA X-act) system was used to image the fracture surfaces of the samples without prior coating.

The Auger Electron Spectroscopy (AES) analyses were carried out with a JEOL JAMP 9500F Auger spectrometer (JEOL Ltd, Tokyo, Japan) working under UHV conditions (pressure < 2.10 Pa - 7 Pa). The

UHV equipment was a Schottky field emission Auger electron spectrometer (FE-AES) dedicated to very high spatial resolution (~ 10 nm probe diameter) analysis and high brightness. The hemi-spherical electron analyzer coupled with a multichannel detector (7 channeltrons) offered ideal settings for energy-resolved Auger analysis. For the high-resolution SEM images for the AES analyses, the same equipment working in SEM mode (30 keV, 2 nA, working distance = 23 mm) was used. Before X-ray photoelectron spectroscopy (XPS) and AES analyses, the samples were cross-cut with a JEOL Cross-Polisher (JEOL Ltd.) by the ion-milling polishing method. One-half of a sample was protected by a stainless steel shield plate and the non-protected area was etched with an Ar^+-ion beam (6 keV). A very clean polished surface was obtained due to the grazing angle (~ 2° to the surface), leading to limited implantation of Ar^+ ions in the etched sample. After cutting and etching, the samples were mounted on a sample holder for Auger analyses.

XPS studies were performed using an ESCALAB 250 Xi spectrometer with a monochromatic Al-Kα X-ray source (hυ = 1486.6 eV). The analysis of a 650 µm × 650 µm area of the sample was completed using a pass energy of 20 eV and a 0.1 eV energy step for the core peaks. An electron flood gun was used for charge compensation. The quantifications were carried out, after Shirley-type background subtraction, by utilizing the Thermo Fisher Scientific Advantage cross-section database. Valence spectra were recorded from -5 eV to 40 eV with a 40 eV pass energy and a 0.2 eV energy step.

The electrical conductivity and Seebeck coefficient were measured simultaneously by ULVAC ZEM-3 in a low-pressure He atmosphere with temperatures varying from a high of 1000 K to a low of 373 K. Thermal diffusivity was measured from 373 K to 1000 K in a vacuum (Netzsch LFA457). The thermal diffusivity measurements at each temperature resulted from averaging three repeated measurements. The specific heat capacity was measured from room temperature up to 1000 K, with a heating rate of 20 $K.min^{-1}$ in platinum crucibles in a nitrogen atmosphere (NETZSCH STA449 F3 Jupiter).

Results and discussion

The undoped CoO was sintered using different sintering temperatures and dwell times in order to obtain a high relative density. For a dwell time of 5 min, relative densities of 85% and 88% were obtained at sintering temperatures of 1223 K and 1273 K, respectively. By extending the dwell time to 10 min at 1273 K, a relative density of 97% was obtained. $Co_{1-x}Na_xO$ (x = 0, 0.01, 0.03, 0.05, and 0.07) pellets were sintered at a lower temperature of 1223 K for 10 min and possessed relative densities of 97%, 96%, 91%, 95%, and 89% respectively. A white powder was observed on the dies and spacers after SPS of Na doped CoO samples. According to the EDS analysis, this white powder is rich in Na. It was also notable that $Co_{1-x}Na_xO$ with x = 0.07 was cracked during SPS, possibly due to the increased amount of evaporation of Na in $Co_{1-x}Na_xO$ with high Na content. Thus, the composition with x = 0.07 exhibited lower relative density than the other samples.

Fig. 1 shows the XRD patterns of $Co_{1-x}Na_xO$ ($0 \leq x \leq 0.07$) pellets. All diffraction peaks can be assigned to CoO with a cubic crystal structure and a space group *Fm-3m* (PDF 01-071-1178). Moreover, pure $Co_{1-x}Na_xO$ has been obtained both after heat treatment and after SPS, indicating the absence of phase change during SPS despite the evaporation of Na. The Rietveld refinement analysis shows that the lattice parameter of undoped CoO is a = 4.262 (3) Å. It remains unchanged with increasing Na content despite the large difference in the ionic radius between Na^+ and Co^{2+}. This could be explained by two aspects: (1) the actual Na dopant concentrations are less than the nominal values and (2) it is possible that Co^{3+} ions were generated as a result of charge compensation. The substitution of Co^{2+} with Na^+ introduces extra charges (holes), and, as a result, Co^{3+} ions are likely to form to maintain the charge neutrality. Indeed, the ionic radius of Na^+ (1.02 Å) is larger than Co^{2+} (high spin: 0.745 Å) in the 6-coordination [40]. However, the ionic radius of Co^{3+} (low spin: 0.545 Å and high spin: 0.61 Å in the 6-coordination [40]) is smaller than that of both Na^+ and Co^{2+}. Thus, Na substitution results in an unchanged lattice parameter.

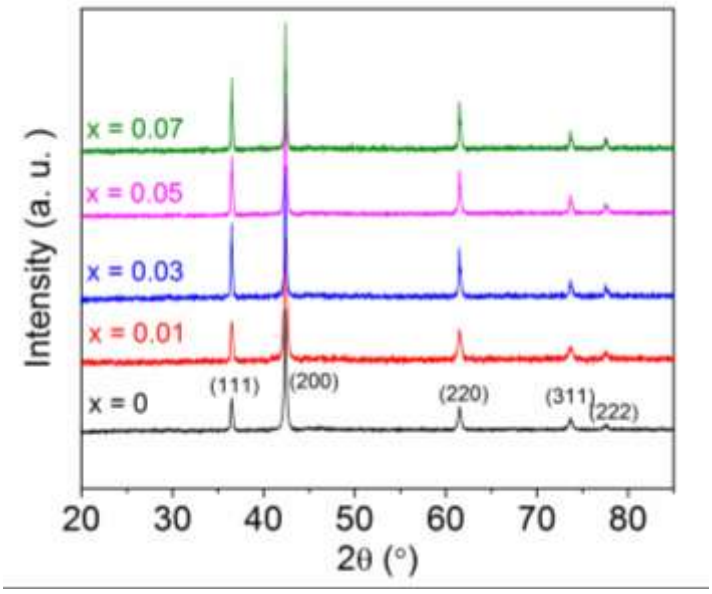

Fig. 1 XRD patterns of $Co_{1-x}Na_xO$ (x = 0, 0.01, 0.03, 0.05 and 0.07) pellets after SPS.

Fig. 2a and b show the Raman spectra of $Co_{1-x}Na_xO$ ceramics at room temperature and 80 K, respectively. At room temperature, the undoped CoO shows broad bands centred at about 530 cm^{-1} and 1060 cm^{-1}. The weak sharp peak around 200 cm^{-1} is associated with spinel Co_3O_4, probably due to incomplete reduction of Co_3O_4 during synthesis. The broad bands near 530 cm^{-1} and 1060 cm^{-1} are attributed to the first-order and second-order Raman scattering, respectively. As mentioned above, CoO adopts a NaCl-type structure in which the first-order Raman scattering is forbidden, while the second-order Raman scattering is allowed [41]. Indeed, Co and O ions in the structures are located at a centre of inversion symmetry, and the optic Raman modes at zone centre do not give rise to a first-order change in the electronic polarizability. The observation of the first-order Raman scattering corresponds to the infrared modes of CoO activated by disorders related to cobalt vacancies and/or other structural defects

in CoO [42-44]. With the addition of Na, the broad band near 530 cm^{-1} splits into sharper peaks at 390, 450, 516 and 560 cm^{-1}, which could indicate an increased degree of lattice disorder. At 80 K, in addition to the bands observed at room temperature, three peaks are visible below 400 cm^{-1} (at 133, 221 and 294 cm^{-1}) for the samples with x = 0 and 0.01. These peaks are associated with the magnetic excitations corresponding to the scattering from magnons. The magnons are related to the antiferromagnetic order in CoO occurring below the Néel temperature (T_N = 292 K) [45]. With increasing Na content, these peaks become weaker and finally disappear, indicating the loss of magnetic ordering and the successful substitution of Na into the crystal lattice of CoO.

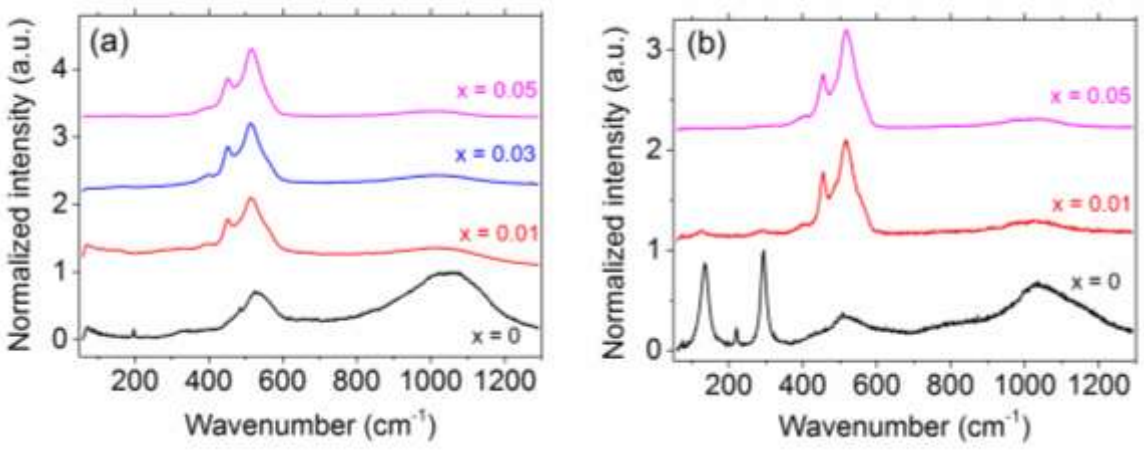

Fig. 2 Raman spectra of $Co_{1-x}Na_xO$ ($0 \leq x \leq 0.05$) ceramics at (a) room temperature and (b) 80 K.

The Na content in the ceramics was measured by flame atomic absorption spectroscopy. With increasing nominal Na content in $Co_{1-x}Na_xO$ (x = 0.01, 0.03, 0.05, and 0.07), the measured Na content was 0, 0.018, 0.036, and 0.054, respectively. Each composition shows a lower Na content than the nominal value, indicating a loss of Na during the heat treatment and SPS processes. This agrees well with the observation of the white powder on the graphite spacers after SPS.

Fig. 3 shows a typical SEM micrograph of $Co_{1-x}Na_xO$ with x = 0.05. AES was undertaken to analyse the chemical composition and element distribution of the sample with x = 0.05. The element distribution maps exhibit a uniform distribution of Co and O on the cross-section of $Co_{1-x}Na_xO$ ceramics. However, rich Na regions located in close vicinity of pores have been detected due to the volatilization observed during SPS. Therefore, the actual amount of Na dopants in the CoO ceramics is lower than the nominal value and the value measured by the bulk chemistry method.

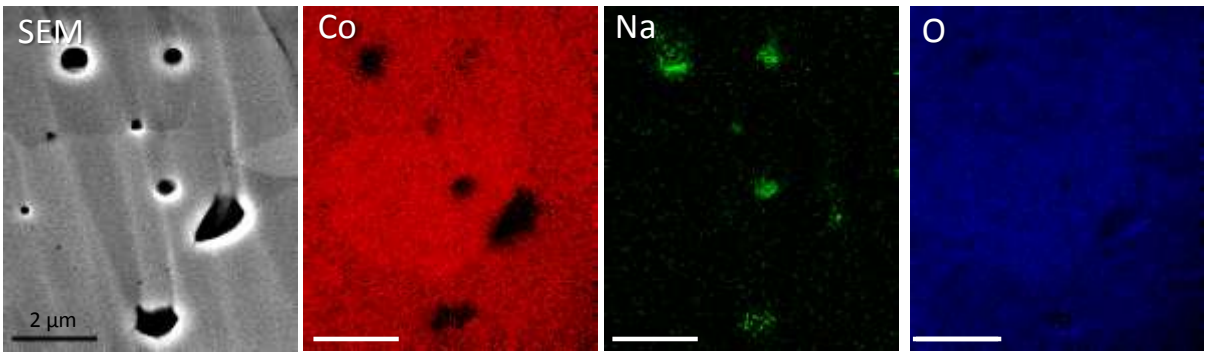

Fig. 3 SEM image and AES mapping images for Co, Na, and O of $Co_{1-x}Na_xO$ with x = 0.05.

The chemical composition and oxidation state of cations in $Co_{1-x}Na_xO$ ceramic with x = 0 and 0.05 were investigated by XPS. The Co 2p core peaks are shown in Fig. 4a. The spectra consist of two main components, Co $2p_{3/2}$ and Co $2p_{1/2}$, located at 780.2 eV and 796.5 eV, respectively. There is also a strong satellite at about 6 eV higher than each binding energy (B. E.). This is a character of cobalt in the divalent state [46, 47]. The presence of a main line together with a satellite peak (shake-up) results from a ligand-to-metal charge transfer during the photoemission process. The O 1s core peaks in Fig. 4b can be decomposed into two components at 529.9 eV and 531.4 eV. These components correspond to Co-O and to carbonates and adsorbed species environments, respectively. The C 1s signal is dominated by the carbon contamination always observed in XPS [48]. As shown in Fig. 4a, the overall shape of the Co 2p core peak is retained for the Na-doped sample. This indicates that the Na insertion does not affect the local electronic structure of Co. Indeed, neither the Co 2p binding energy nor the area ratio between the satellite and the main peak indicate an evolution of the oxidation state. Van Elp et al. [46] have reported that even for CoO doped with 20% of Li, the Co 2p remained identical. On the other hand, the main component of the Na 1s core peak at 1072 eV (Fig. 4c) can be assigned to Na in carbonate environment, which is consistent with the intensity increase in the O 1s component at 531.5 eV [49]. The smallest component (B. E. (Na 1s) = 1069.8 eV) could be correlated to the substitution of Na into the CoO structure. Thus, only an extremely weak part of sodium is doped into CoO. Fig. 4d shows the valence band of the two samples. Na substitution does not impact the broad range of the valence band region relative to the Co 3d contribution [46]. For the doped sample, we can identify the Na 2p core peak at 31.1 eV. Table 1 shows that the compositions obtained from XPS analyses are $CoO_{0.79}$ for the non-doped and $Na_{0.01}Co_{0.99}O_{0.73}$ for the 5% Na-doped sample.

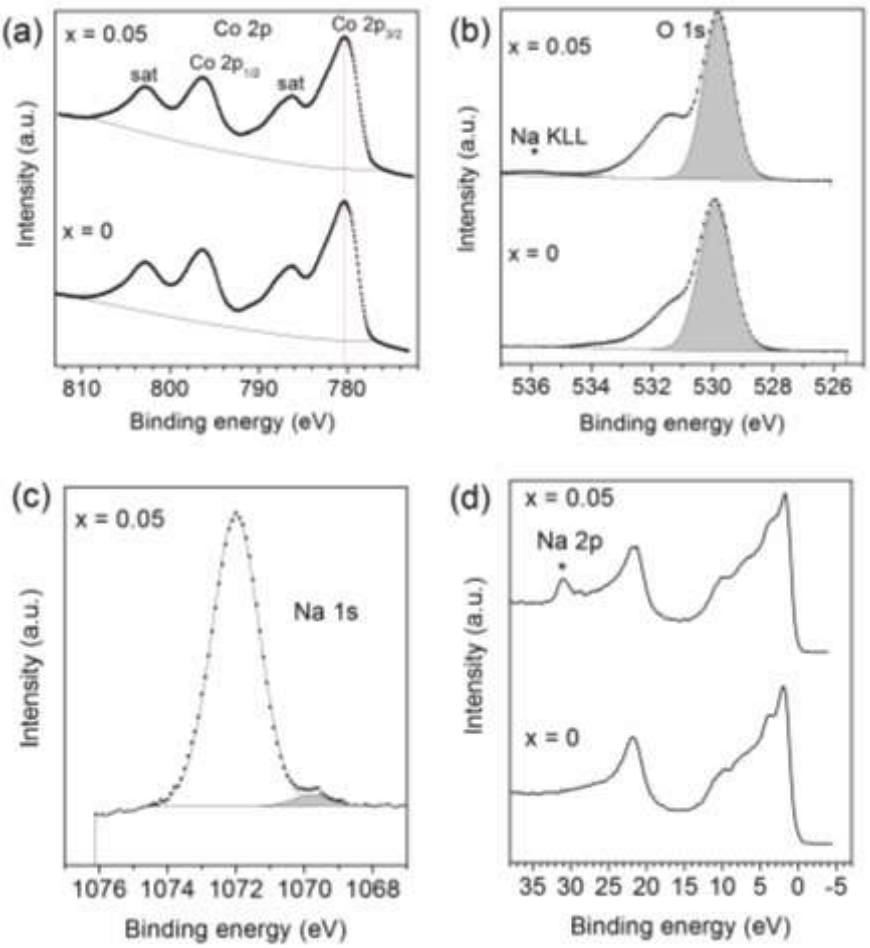

Fig. 4 XPS spectra of $Co_{1-x}Na_xO$ (x = 0 and 0.05) ceramics. (a) Co 2p core peaks, (b) O 1s core peaks, (c) Na 1s core peaks, and (d) valence bands.

Table 1 Atomic percentages (%) of the Co, O, C, and Na elements in $Co_{1-x}Na_xO$ (x = 0 and 0.05) ceramics obtained from XPS.

	x = 0	**x = 0.05**
	at. %	at. %
Co 2p$_{3/2}$	**35.1**	**37.1**
O 1s *(oxide)*	27.7	26.9
O 1s *(other species)*	11.1	14.9
O 1s total	**38.9**	**41.8**
C 1s	**26.0**	**18.1**
Na 1s *(substitution)*		0.4
Na 1s *(carbonate)*		2.3
Na 1s total		**2.7**

Fig. 5 shows the thermoelectric properties of $Co_{1-x}Na_xO$. Some samples show incomplete measurement over the full range of temperature due to the limitations of the instrument. The electrical conductivity (Fig. 5a) of $Co_{1-x}Na_xO$ increases with increasing temperature, showing semiconducting behaviour. The highly resistive undoped CoO exhibits an insulating nature and a low concentration of charged Co

vacancies. The electrical conductivity increases abruptly with increasing Na content until $x = 0.05$, even though the actual concentrations of Na dopant are far less than the nominal values according to XPS. At 1000 K, the electrical conductivity is remarkably increased from 33 $S.m^{-1}$ to 4096 $S.m^{-1}$ as Na content increases from 0 to 0.05. A similar observation has also been reported in In_2O_3 doped with extremely small amounts of Ti [51]. The decrease in electrical conductivity for the sample with $x = 0.07$ is probably due to the presence of cracks.

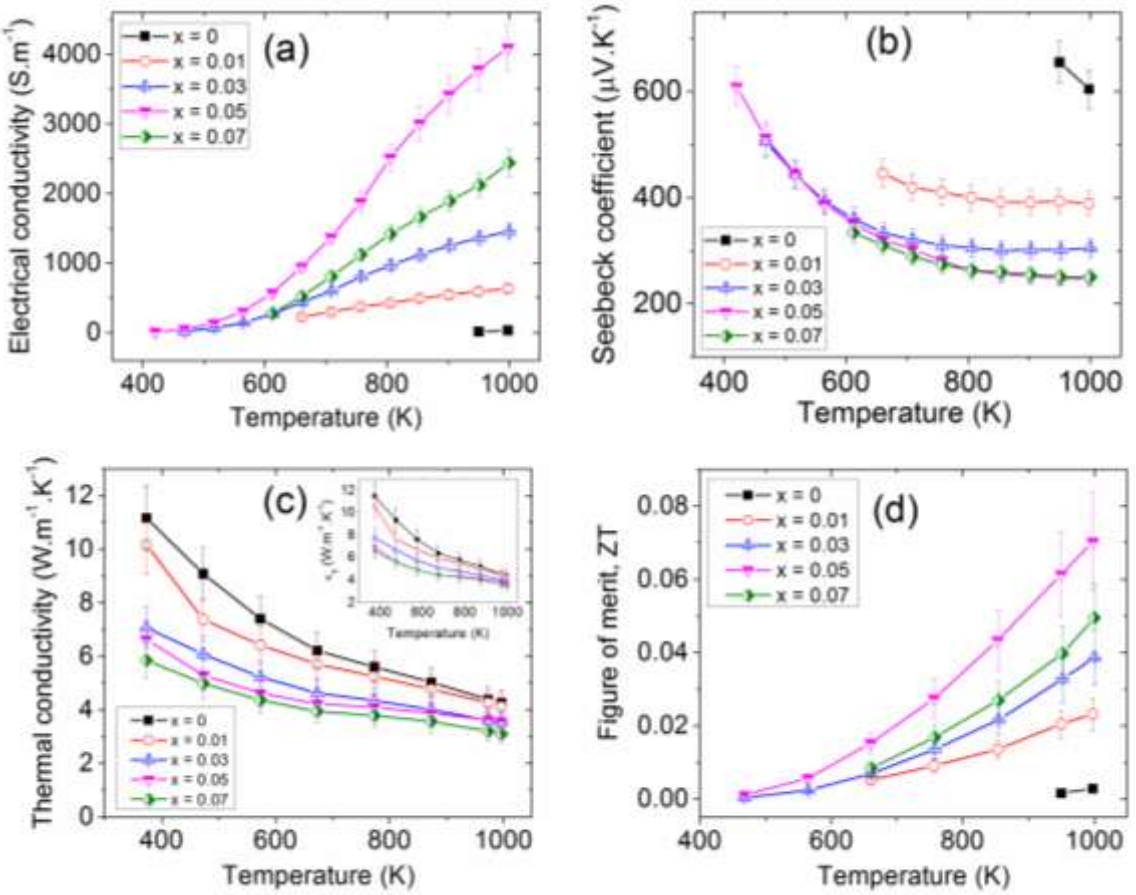

Fig. 5 Thermoelectric properties of $Co_{1-x}Na_xO$ (x = 0, 0.01, 0.03, 0.05, and 0.07) ceramics as a function of temperature. (a) Electrical conductivity, (b) Seebeck coefficient, (c) thermal conductivity, and (d) figure of merit, *ZT*. The insert in (c) shows the solid thermal conductivity (κ_s) at zero porosity calculated from the measured thermal conductivity κ ($\kappa_s = \kappa$ / relative density [50]).

The positive Seebeck coefficient (Fig. 5b) indicates that all compositions are p-type semiconductors. The Seebeck coefficient decreases with increasing temperature. Above 650 K, the Seebeck coefficient of $Co_{1-x}Na_xO$ decreases with increasing Na content up to $x = 0.05$ and remains unchanged with a further increase in x. With the addition of Na, the carrier concentration is increased, leading to an increase in the electrical conductivity and a decrease in the Seebeck coefficient. No obvious change is observed in the Seebeck coefficient in $Co_{1-x}Na_xO$ with $x \geq 0.05$, indicating a saturation of Na content in CoO around 0.05. The power factor ($S^2\sigma$) can be calculated from the Seebeck coefficient and electrical conductivity.

$Co_{1-x}Na_xO$ with $x = 0.05$ exhibits the highest power factor of 250 $\mu W.m^{-1}.K^{-2}$ at 1000 K. This high value is similar to the power factor of $Ca_3Co_4O_9$ [10, 52] and, thus, indicates that the material could be a promising thermoelectric oxide.

The thermal conductivity (Fig. 5c) of $Co_{1-x}Na_xO$ decreases with increasing temperature. Due to the different relative densities between the samples, the solid thermal conductivity is calculated and shown in the insert of Fig. 5c. The solid thermal conductivity decreases with increasing Na content until $x = 0.05$, possibly due to increased lattice disorder, which has been confirmed by Raman scattering. Fig. 5d shows that *ZT* increases with increasing temperature for all samples and it is considerably enhanced by substituting Co^{2+} with Na^+, reaching 0.07 at 1000 K for $x = 0.05$. This *ZT* value is comparable to that of the Li and Na co-doped NiO with a similar temperature, which exhibits a value of $ZT \sim 0.06$ at 1060 K [20].

The addition of Ag rather than Na to CoO leads to very different behaviour. Ag forms particles within the CoO matrix, indicating the limited incorporation of Ag^+ into Co^{2+} sites. For $Co_{1-x}Ag_xO$ with $x = 0.01$, the thermoelectric properties are unchanged compared to the undoped CoO, exhibiting a $ZT \sim 0.003$ at 1000 K. The composition with $x = 0.05$ exhibits lower electrical conductivity and Seebeck coefficient and higher thermal conductivity than the undoped CoO. Thus, its highest *ZT* is only 0.001 at 1000 K. With such negative impact on the thermoelectric properties, characterizations are not further presented.

Conclusions

$Co_{1-x}Na_xO$ ($0 \leq x \leq 0.07$) and $Co_{1-x}Ag_xO$ ($0 \leq x \leq 0.05$) ceramics have been prepared by heat treatment and spark plasma sintering. While a pure-phase material with a rock-salt structure has been obtained for Na-doped CoO, a CoO/Ag-composite material was obtained for Ag-doped CoO. An evaporation of Na during the synthesis of Na-doped CoO has also been confirmed. XPS of the Na-doped CoO shows no change in the local electronic structure of Co 2p and confirms that the amount of effective Na dopants is much smaller than the nominal value. The carrier concentration is increased with increasing Na content, leading to a remarkable enhancement in the electrical conductivity and a decrease in the Seebeck coefficient. The highest power factor of $Co_{1-x}Na_xO$ was ~ 250 $\mu W.m^{-1}.K^{-2}$ at 1000 K for the composition with $x = 0.05$, indicating that it could serve as promising p-type thermoelectric oxide in the future. The degree of lattice disorder in CoO was found to increase as a result of Na doping, resulting in a reduction in the thermal conductivity of the material. Thus, a *ZT* of ~ 0.07 at 1000 K has been achieved in $Co_{0.95}Na_{0.05}O$. However, the *ZT* was found to decrease when Ag was added into CoO. The thermoelectric properties of CoO could be further optimized by co-doping other monovalent cations, nanostructuring, and improving synthesis methods.

References

1. Snyder, G.J. and E.S. Toberer, *Complex thermoelectric materials.* Nat Mater, 2008. **7**(2): p. 105-114.

2. Shi, X., J. Yang, J.R. Salvador, M. Chi, J.Y. Cho, H. Wang, S. Bai, J. Yang, W. Zhang, and L. Chen, *Multiple-filled skutterudites: high thermoelectric figure of merit through separately optimizing electrical and thermal transports.* J. Amer. Chem. Soc., 2011. **133**(20): p. 7837-7846.
3. Saramat, A., G. Svensson, A.E.C. Palmqvist, C. Stiewe, E. Mueller, D. Platzek, S.G.K. Williams, D.M. Rowe, J.D. Bryan, and G.D. Stucky, *Large thermoelectric figure of merit at high temperature in Czochralski-grown clathrate $Ba_8Ga_{16}Ge_{30}$.* J. Appl. Phys., 2006. **99**(2): p. 023708.
4. Kenjiro, F., M. Tadashi, and N. Kazuo, *High-Temperature Thermoelectric Properties of $Na_xCoO_{2-\delta}$ Single Crystals.* Jpn. J. Appl. Phys., 2001. **40**(7R): p. 4644.
5. Shikano, M. and R. Funahashi, *Electrical and thermal properties of single-crystalline $(Ca_2CoO_3)_{0.7}CoO_2$ with a $Ca_3Co_4O_9$ structure.* Appl. Phys. Lett., 2003. **82**(12): p. 1851-1853.
6. Funahashi, R. and M. Shikano, *$Bi_2Sr_2Co_2O_y$ whiskers with high thermoelectric figure of merit.* Appl. Phys. Lett., 2002. **81**(8): p. 1459-1461.
7. Van Nong, N., N. Pryds, S. Linderoth, and M. Ohtaki, *Enhancement of the Thermoelectric Performance of p-Type Layered Oxide $Ca_3Co_4O_{9+\delta}$ Through Heavy Doping and Metallic Nanoinclusions.* Adv. Mater., 2011. **23**(21): p. 2484-2490.
8. Funahashi, R., I. Matsubara, and S. Sodeoka, *Thermoelectric properties of $Bi_2Sr_2Co_2O_x$ polycrystalline materials.* Appl. Phys. Lett., 2000. **76**(17): p. 2385-2387.
9. Wang, Y., Y. Sui, X. Wang, W. Su, and X. Liu, *Enhanced high temperature characteristics of transition metals doped $Ca_3Co_4O_{9+\delta}$ by cold high-pressure fabrication*. J. Appl. Phys., 2010. 107: p. 033708-033708.
10. Delorme, F., C.F. Martin, P. Marudhachalam, D. Ovono Ovono, and G. Guzman, *Effect of Ca substitution by Sr on the thermoelectric properties of $Ca_3Co_4O_9$ ceramics.* J. Alloys Compd., 2011. **509**(5): p. 2311-2315.
11. Tian, R., R. Donelson, C.D. Ling, P.E.R. Blanchard, T. Zhang, D. Chu, T.T. Tan, and S. Li, *Ga substitution and oxygen diffusion kinetics in $Ca_3Co_4O_{9+\delta}$-based thermoelectric oxides.* J. Phys. Chem. C, 2013. **117**(26): p. 13382-13387.
12. Wang, Y., Y. Sui, J. Cheng, X. Wang, and W. Su, *Comparison of the high temperature thermoelectric properties for Ag-doped and Ag-added $Ca_3Co_4O_9$.* J. Alloys Compd., 2009. **477**(1): p. 817-821.
13. Chen, C., T. Zhang, R. Donelson, D. Chu, R. Tian, T.T. Tan, and S. Li, *Thermopower and chemical stability of $Na_{0.77}CoO_2/Ca_3Co_4O_9$ composites.* Acta Mater., 2014. **63**: p. 99-106.
14. Saini, S., H.S. Yaddanapudi, K. Tian, Y. Yin, D. Magginetti, and A. Tiwari, *Terbium Ion Doping in $Ca_3Co_4O_9$: A Step towards High-Performance Thermoelectric Materials.* Sci. Rep., 2017. **7**: p. 44621.
15. Koshibae, W., K. Tsutsui, and S. Maekawa, *Thermopower in cobalt oxides.* Phys. Rev. B, 2000. **62**(11): p. 6869-6872.
16. Kozuka, H., H. Yamada, T. Hishida, K. Yamagiwa, K. Ohbayashi, and K. Koumoto, *Electronic transport properties of the perovskite-type oxides $La_{1-x}Sr_xCoO_{3\pm\delta}$.* J. Mater. Chem., 2012. **22**(38): p. 20217-20222.
17. Chen, C., F. Giovannelli, T. Chartier, and F. Delorme, *Synthesis and thermoelectric properties of doubly substituted $La_{0.95}Sr_{0.05}Co_{1-x}Cr_xO_3$ ($0 \leq x \leq 0.5$).* Mater. Res. Bull., 2018. **102**: p. 257-261.
18. Bousnina, M.A., R. Dujardin, L. Perriere, F. Giovannelli, G. Guegan, and F. Delorme, *Synthesis, sintering, and thermoelectric properties of the solid solution $La_{1-x}Sr_xCoO_{3\pm\delta}$ ($0 \leqslant x \leqslant 1$).* Journal of Advanced Ceramics, 2018.
19. Delorme, F., C. Chen, B. Pignon, F. Schoenstein, L. Perriere, and F. Giovannelli, *Promising high temperature thermoelectric properties of dense $Ba_2Co_9O_{14}$ ceramics.* J. Eur. Ceram. Soc., 2017. **37**(7): p. 2615-2620.
20. Shin, W. and N. Murayama, *High performance p-type thermoelectric oxide based on NiO.* Mater. Lett., 2000. **45**(6): p. 302-306.
21. Zhang, L.Y. and D.S. Xue, *Preparation and magnetic properties of pure CoO nanoparticles.* J. Mater. Sci. Lett., 2002. **21**(24): p. 1931-1933.

22. Yang, H.M., J. Ouyang, and A.D. Tang, *Single step synthesis of high-purity CoO nanocrystals.* J. Phys. Chem. B, 2007. **111**(28): p. 8006-8013.
23. Kundu, S., A.J. Nelson, S.K. McCall, T. van Buuren, and H. Liang, *Shape-influenced magnetic properties of CoO nanoparticles.* J. Nanopart. Res., 2013. **15**(5).
24. Jena, A., T.R. Penki, N. Munichandraiah, and S.A. Shivashankar, *Flower-like porous cobalt(II) monoxide nanostructures as anode material for Li-ion batteries.* J. Electroanal. Chem., 2016. **761**: p. 21-27.
25. Fisher, B. and D.S. Tannhauser, *Electrical properties of cobalt monoxide.* J. Chem. Phys., 1966. **44**(4): p. 1663-1672.
26. Joshi, G.M., M. Pai, H.R. Harrison, C.J. Sandberg, R. Aragon, and J.M. Honig, *Electrical properties of undoped single CoO crystals.* Mater. Res. Bull., 1980. **15**(11): p. 1575-1579.
27. Koumoto, K., K. Yamayoshi, and H. Yanagida, *Electrical conduction in $Co_{1-x}Mg_xO$.* J. Am. Ceram. Soc., 1983. **66**(1): p. 42-45.
28. Petot-Ervas, G., P. Ochin, and B. Sossa, *Transport properties in pure and lithium-doped cobaltous oxide.* Solid State Ionics, 1984. **12**: p. 277-293.
29. Borchardt, G., K. Kowalski, J. Nowotny, M. Rekas, and W. Weppner, *Thermopower and electrical conductivity of single crystal and polycrystalline CoO.* J. Eur. Ceram. Soc., 1994. **14**(4): p. 369-376.
30. Borchardt, G., K. Kowalski, J. Nowotny, M. Rekas, and W. Weppner, *Electrical properties of undoped CoO - A Debye-Huckel approach.* J. Mater. Sci., 1996. **31**(19): p. 5185-5190.
31. Iguchi, E., T. Hashimoto, and S. Yokoyama, *Electrical transports and stability of small polarons of O 2p holes in $Li_xCo_{1-x}O$.* J. Phys. Soc. Jpn., 1996. **65**(1): p. 221-229.
32. Bosman, A.J. and H.J. Vandaal, *Small-polaron versus band conduction in some transition-metal oxides.* Adv Phys., 1970. **19**(77): p. 1-117.
33. Chen, H.C., E. Gartstein, and T.O. Mason, *Conduction mechanism analysis for $Fe_{1-\delta}O$ and $Co_{1-\delta}O$.* J. Phys. Chem. Solids, 1982. **43**(10): p. 991-995.
34. Logothetis, E.M. and J.K. Park, *High temperature electrical properties and defect structure of $Co_{1-x}Mg_xO$.* J. Phys. Chem. Solids, 1986. **47**(2): p. 193-200.
35. Chen, H.C. and T.O. Mason, *Thermoelectric study of cobaltous oxide defect structure.* J. Am. Ceram. Soc., 1981. **64**(10): p. C130-C133.
36. Khowash, P.K. and D.E. Ellis, *Nature of defect structure in CoO.* Phys. Rev. B, 1987. **36**(6): p. 3394-3399.
37. Wdowik, U.D., *Ab initio study of point defects in the strongly correlated system CoO.* Phys. Rev. B, 2011. **84**(6): p. 064111.
38. Constant, K.P., T.O. Mason, S.J. Rothman, and J.L. Routbort, *Non-stoichiometry, electrical properties, and cation diffusion in highly nonstoichiometric $Co_{1-x}O$. 1. Experimental.* J. Phys. Chem. Solids, 1992. **53**(3): p. 405-411.
39. Rodríguez-Carvajal, J., *Recent developments of the program FULLPROF.* Commission on powder diffraction (IUCr). Newsletter, 2001. **26**: p. 12-19.
40. Shannon, R., *Revised effective ionic radii and systematic studies of interatomic distances in halides and chalcogenides.* Acta Crystallogr., Sect. A, 1976. **32**(5): p. 751-767.
41. Singh, R.K., *Many body interactions in binary ionic solids.* Phys. Rep., 1982. **85**(5): p. 259-401.
42. Li, Y., W. Qiu, F. Qin, H. Fang, V.G. Hadjiev, D. Litvinov, and J. Bao, *Identification of cobalt oxides with Raman scattering and Fourier transform infrared spectroscopy.* J. Phys. Chem. C, 2016. **120**(8): p. 4511-4516.
43. Rivas-Murias, B. and V. Salgueiriño, *Thermodynamic $CoO–Co_3O_4$ crossover using Raman spectroscopy in magnetic octahedron-shaped nanocrystals.* J. Raman Spectrosc., 2017. **48**(6): p. 837-841.
44. Gielisse, P.J., J.N. Plendl, L.C. Mansur, R. Marshall, S.S. Mitra, R. Mykolajewycz, and A. Smakula, *Infrared properties of NiO and CoO and their mixed crystals.* J. Appl. Phys., 1965. **36**(8): p. 2446-2450.
45. Chou, H.h. and H.Y. Fan, *Light scattering by magnons in CoO, MnO, and α-MnS.* Phys. Rev. B, 1976. **13**(9): p. 3924-3938.

46. van Elp, J., J.L. Wieland, H. Eskes, P. Kuiper, G.A. Sawatzky, F.M.F. de Groot, and T.S. Turner, *Electronic structure of CoO, Li-doped CoO, and $LiCoO_2$.* Phys. Rev. B, 1991. **44**(12): p. 6090-6103.
47. Biesinger, M.C., B.P. Payne, A.P. Grosvenor, L.W.M. Lau, A.R. Gerson, and R.S.C. Smart, *Resolving surface chemical states in XPS analysis of first row transition metals, oxides and hydroxides: Cr, Mn, Fe, Co and Ni.* Appl. Surf. Sci., 2011. **257**(7): p. 2717-2730.
48. Andreu, N., D. Flahaut, R. Dedryvere, M. Minvielle, H. Martinez, and D. Gonbeau, *XPS Investigation of Surface Reactivity of Electrode Materials: Effect of the Transition Metal.* ACS Appl. Mater. Interfaces, 2015. **7**(12): p. 6629-6636.
49. Zhang, B., G. Rousse, D. Foix, R. Dugas, D.A.D. Corte, and J.M. Tarascon, *Microsized Sn as Advanced Anodes in Glyme‐Based Electrolyte for Na‐Ion Batteries.* Adv. Mater., 2016. **28**(44): p. 9824-9830.
50. Kingery, W.D., J. Francl, R.L. Coble, and T. Vasilos, *Thermal conductivity: X, data for several pure oxide materials corrected to zero porosity.* J. Am. Ceram. Soc., 1954. **37**(2): p. 107-110.
51. Guilmeau, E., D. Berardan, C. Simon, A. Maignan, B. Raveau, D.O. Ovono, and F. Delorme, *Tuning the transport and thermoelectric properties of In_2O_3 bulk ceramics through doping at In-site.* J. Appl. Phys., 2009. **106**(5): p. 7.
52. Kenfaui, D., G. Bonnefont, D. Chateigner, G. Fantozzi, M. Gomina, and J.G. Noudem, *$Ca_3Co_4O_9$ ceramics consolidated by SPS process: Optimisation of mechanical and thermoelectric properties.* Mater. Res. Bull., 2010. **45**(9): p. 1240-1249.